J Electr Eng Technol.2017; 12(5): 1891-1901
http://doi.org/10.5370/JEET.2017.12.5.1891

ISSN(Print) 1975-0102
ISSN(Online) 2093-7423

Efficiency Improvement of Synchronous Boost Converter with Dead Time Control for Fuel Cell-Battery Hybrid System

Do-Yun Kim*, Il-Kuen Won, Jung-Hyo Lee† and Chung-Yuen Won****

Abstract – In this paper, optimal control of the fuel cell and design of a high-efficiency power converter is implemented to build a high-priced fuel cell system with minimum capacity. Conventional power converter devices use a non-isolated boost converter for high efficiency while the battery is charged, and reduce its conduction loss by using MOSFETs instead of diodes. However, the efficiency of the boost converter decreases, since overshoot occurs because there is a moment when the body diode of the MOSFET is conducted during the dead time and huge loss occurs when the dead time for the maximum-power-flowing state is used in the low-power-flowing state. The method proposed in this paper is to adjust the dead time of boost and rectifier switches by predicting the power flow to meet the maximum efficiency in every load condition. After analyzing parasite components, the stability and efficiency of the high-efficiency boost converter is improved by predictive compensation of the delay component of each part, and it is proven by simulation and experience. The variation in switching delay times of each switch of the full-bridge converter is compensated by falling time compensation, a control method of PWM, and it is also proven by simulation and experience.

Keywords: Predictive control of dead time, Synchronous boost converter, High-efficiency fuel cell converter

1. Introduction

There has been much research on the fuel-cell-and-battery hybrid system that endows a fuel cell with long charging time and low energy density of battery [1-4]. Fig. 1 shows that a fuel-cell-and-battery hybrid system is made up of a fuel cell stack, a DC/DC converter that charges the battery, a secondary cell, and an isolated full-bridge DC/DC converter that changes the voltage of the secondary cell to meet output requirements. The DC/DC converter charges the battery with fuel cell power to minimize the capacity of expensive fuel cells, and thus a non-isolated DC/DC converter should be selected over an isolated DC/DC converter, which is of low efficiency. In this study, 50 PEM fuel cells (35-42 V) and, as the secondary cell, a lithium battery equivalent to 13 fuel cells (43-52 V) were used, making the use of a boost converter a necessity.

The DC/DC converter of a fuel cell system should feature a MOSFET instead of an IGBT, to achieve high efficiency as a converter [8-13].

A non-isolated converter is used; in general, a boost converter that uses a diode like Fig. 2. A diode boost converter undergoes substantial current loss from the conduction loss, and reverse recovery time caused by the diode. To achieve high efficiency, a synchronous boost converter that uses a power switch instead of a diode is required [5-7].

A Synchronous Boost converter has higher switching losses than boost converters that uses a diode, but results in better efficiency because the MOSFET switching losses are lower in the low current region. However, due to the

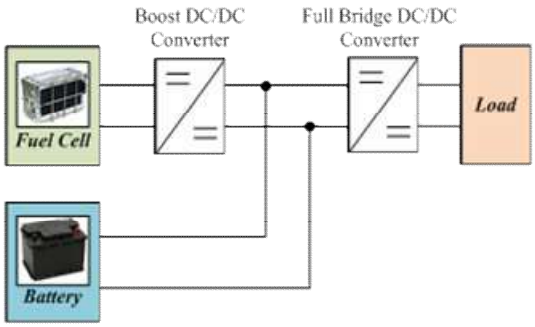

Fig. 1. Configuration of a fuel-cell-and-battery hybrid system

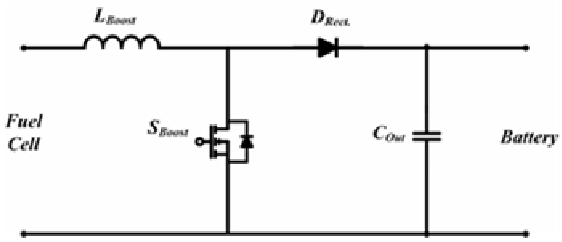

Fig. 2. Boost converter using diode

† Corresponding Author: Dept. of Electrical Engineering, Kunsan National University, Korea. (jhlee82@kunsan.ac.kr)
* Dept. of vehicle components company, LG Electronics, Korea. (doyun1279.kim@lge.com)
** Dept. of Electrical and Computer Engineering, Sungkyunkwan University, Korea. ({woncy,ganzipers}@skku.edu)
Received: September 9, 2016; Accepted: May 28, 2017

characteristics of the fuel cell which is a low voltage, high current type, it is expected that the application of the synchronous boost converter in the fuel cell application will have a great effect in terms of efficiency.

Fig. 3 shows that a synchronous boost converter that uses a MOSFET has a power switch consisting of a boost MOSFET (S_{Boost}) and a rectification MOSFET (S_{Rect}). The input and output voltage and current of the synchronous booster converter are sensed for protection from over-voltage and over-current. In keeping with the generative capacity resulting from the hydrogen in the fuel cells, the converter limits input current, but does not control output voltage, to charge the battery with a set amount of power generated by the fuel cells.

This paper shows how to predict the required dead time based on the parasitic component of the switching element in the synchronous boost converter of a fuel-cell-and-battery hybrid system, to achieve higher efficiency by controlling the dead time according to power levels [14, 15].

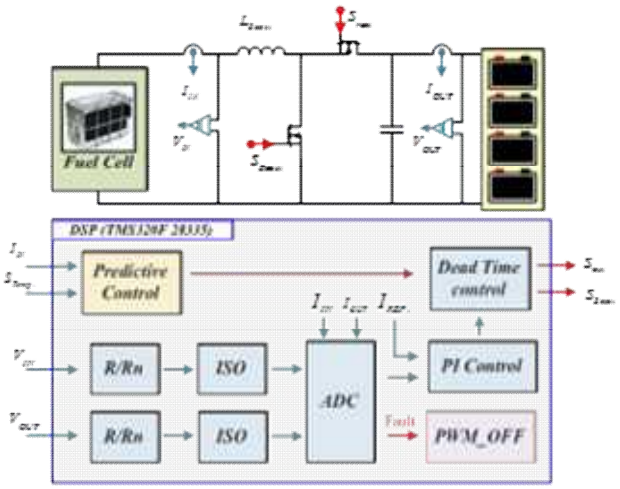

Fig. 3. Configuration of a synchronous boost converter

Fig. 4 (a) shows the current flow when SBoost of the synchronous boost converter is turned on. While S_{Boost} is turned on, L_{Boost} is charged and energy stored in C_{OUT} is transferred to the load. Fig. 4 (b) shows the current flow when S_{Boost} is turned off and S_{Rect} is turned on. Energy charged in L_{Boost} is transferred to C_{OUT} and through S_{Rect}.

S_{Boost} and S_{Rect} operate complementarily, and actually dead time is essential considering the time required to turn on and off. This paper shows how to predict the required dead time based on the parasitic component of the switching element in the synchronous boost converter of a fuel-cell-and- battery hybrid system, to achieve higher efficiency by controlling the dead time according to power levels [14, 15].

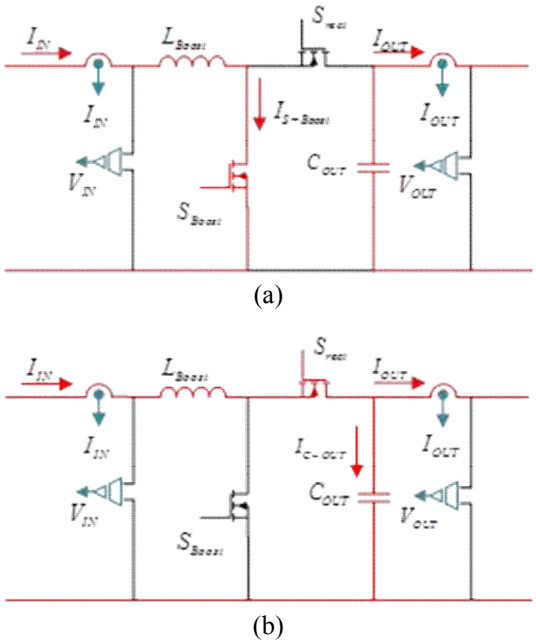

Fig. 4. A synchronous boost converter operation (a) S_{Boost} turn-on (b) S_{Rect} turn-on

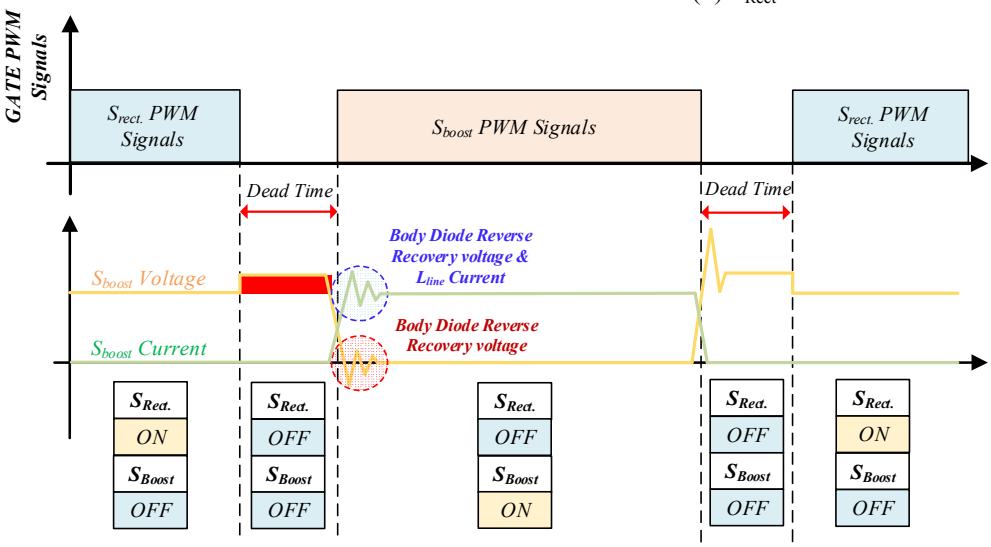

Fig. 5. Waveform of the loss during the dead time

2. Dead Time Loss of a Synchronous Boost Converter

A synchronous boost converter using a MOSFET which has a higher conduction loss than a diode is used to design a DC/DC converter of a low-voltage large current type with a fuel cell characteristic of a low cell voltage. The dead time control of the synchronous boost converter can reduce voltage drop, conduction, and overshoot with Irr characteristic through the body diode of the rectifier switch. The dead time control of the synchronous boost converter which is proposed in paper can compensate the loss by dead time in low output band by controlling the fixed dead time at the maximum power according to the power.

A synchronous boost converter has an S_{BOOST} switch for voltage boost, and an S_{Rect} switch for rectification. These two switches are complementary to each other.

During the switch on-off interval, dead time based on the on-off time delay is set. Too short a dead time causes an arm-short, which leads to an overshot; too long a dead time increases the conduction time of the S_{Rect} Switch, and causes a significant loss. Loss caused by the dead time of a synchronous boost converter becomes manifest as shown in Fig. 5. A longer dead time results in conduction in the body diode of the S_{Rect} switch.

Eq. (1) shows that the first loss occurs from the voltage drop of the diode. The parasitic diode of the MOSFET generates a voltage drop of more than 1.2V, which is 0.4 to 0.7V higher than that of a normal diode

$$P_{loss}(V_f) = V_f \cdot I_L \cdot (T_{dead} \cdot 2) \cdot f_{sw} \quad (1)$$

Eq. (2) shows that the second loss results from Q_{rr}, the voltage loss in the reverse recovery of the diode. The characteristic low-voltage and high current of fuel cell output produces a great loss, even from small voltage loss.

$$P_{loss}(Q_{rr}) = \frac{1}{2} \cdot \frac{temp}{Q_{rr}} \cdot temp \cdot V_{out} \cdot f_{sw} \quad (2)$$

The last loss, current loss from the reverse recovery time of the diode, results from the parasitic component L, between the boost reactor and the S_{Boost}. Eq. (3) shows the extent of loss.

$$P_{loss}(I_{rr}) = \frac{1}{2} \cdot L_{L_{Boost-MOSFET}} \cdot I_{rr}^2 \cdot f_{sw} \quad (3)$$

3. The Proposed Method of Dead Time Control

The PWM dead time required between the switches of a synchronous boost converter is divided into a delay element resulting from the gate driver signals, and a delay element resulting from the parasitic component of the switches and circuits in the power unit.

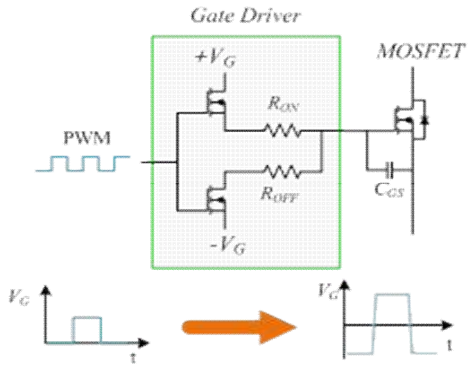

Fig. 6. Gate driver configuration

The proposed dead time control method achieves higher efficiency by identifying a capacitance based on the temperature of C_{DS}, the parasitic component C of the switch element, and selecting a dead time based on the switch temperature to minimize the flow time of S_{Rect} to the body diode. Identifying the ideal dead time requires that the signal level of gate driver PCB, a fixed delay value, be first identified.

Fig. 6 shows the configuration of the gate driver. The minor signal of 5V generated by the DSP is amplified to 15V to drive the MOSFET switch, and requires current to charge the C_{GS}.

To enable quick on-off switching of the MOSFET, the gate driver supplies minus voltage when the switch is turned off, to maximize the discharge speed of C_{GS}. There is on/off resistance that restricts on/off current charging at switch-on and switch-off; delay time is determined by resistance.

The dead time between the switches of a synchronous boost converter that complement each other needs only to accommodate the delay at switch-off, so only the turn-off time for the off-signal voltage of -10V needs to be identified, not the on-signal voltage of 15V. And switch-off; delay time is determined by resistance.

The dead time between the switches of a synchronous boost converter that complement each other needs only to accommodate the delay at switch-off, so only the turn-off time for the off-signal voltage of -10V needs to be identified, not the on-signal voltage of 15V.

Eq. (4) shows how this value can be identified, as well as the discharge time of C_{GS}.

$$T_{OFF} = R_{OFF} \cdot C_{GS} \cdot V_{GS} \quad (4)$$

Table 1 shows that the CGS value changes with the temperature, so identifying an accurate switch-off time requires a capacitance corresponding to the temperature. The on/off times in Table 1 were calculated by using a temperature chamber to send a current of 18A to the 30V of the switch. Dead time of the synchronous boost converter is caused by C_{DS}, which is the parasitic capacitor

Table 1. Capacitance produced by the MOSFET switch temperature

Temp.	C_{GS}	C_{DS}
25 [℃]	75 [nF]	52 [nF]
35 [℃]	68 [nF]	46 [nF]
45 [℃]	57 [nF]	41 [nF]
55 [℃]	45 [nF]	33 [nF]
65 [℃]	36 [nF]	24 [nF]
75 [℃]	25 [nF]	16 [nF]
85 [℃]	15 [nF]	8 [nF]

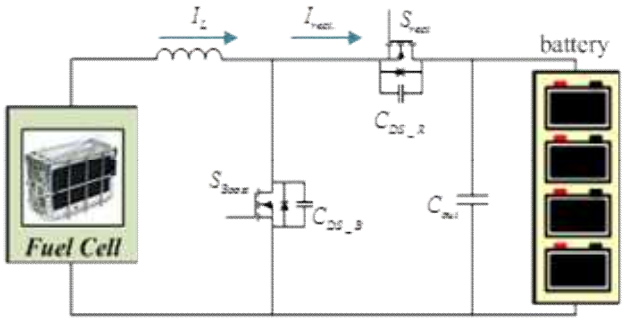

Fig. 7. Component "C" and current flow in a synchronous boost converter

component at each end of the switch drain source, as well as delay caused by the gate.

Fig. 7 shows the parasitic component C and current flow for identifying on/off delay in the power unit of a synchronous boost converter. On/off delay is also caused by C_{DS} of the MOSFET switch, and the charging/discharge current of rectification voltage. Eq. (5) shows switch delay time occurring in the power unit.

$$t_{dead(POWER)} = \frac{C_{DS(S_{Boost})} \cdot V_{Boost}}{I_L} + \frac{C_{DS(S_{Rect.})} \cdot V_{\mathrm{Rect.}}}{I_{\mathrm{Rect.}}} \tag{5}$$

To obtain an accurate final dead time, delay caused by the gate drive and delay caused by the power unit both need to be taken into account.

$$\begin{aligned} t_{dead}(Total) &= \left(\frac{C_{DS(S_{\mathrm{Rect.}})} \cdot V_{\mathrm{Rect.}}}{I_{\mathrm{Rect.}}}\right) + \left(\frac{Q_g}{I_{OFF}}\right) \\ &= \left(\frac{52 \cdot 10^{-9} \cdot 55}{1.7}\right) + \left(\frac{1035 \cdot 10^{-9}}{3}\right) \\ &= (1682 \cdot 10^{-9}) + (310 \cdot 10^{-9}) \\ &= 1.992[\mu S] \end{aligned} \tag{6}$$

The value calculated by the Eq. (6) must be found between synchronous boost converters with dead times of 1.992 μS or higher that are complementary. The synchronous boost converter proposed in this study changes C_{GS} charging capacity according to temperature change for an accurate dead time measurement.

$$\begin{aligned} C_{GS} &= Temp_{MAX} - (temp \cdot \Delta k) \\ \Delta k &= \frac{C_{GS(MAX\ TEMP)}}{Temp_{MAX}} \end{aligned} \tag{7}$$

Δk : G-S capacitance of MOSFET per 1℃

Eq. (7) shows the delay at the gate based on the capacity change in the C_{GS} caused by switch temperature. Eq. (8) shows the temperature change.

$$\begin{aligned} & t_{dead(Total)} \\ &= \left(\frac{(TEMP_{MAX} \cdot 10^N - (temp_{\mathrm{Real}} \cdot \frac{C_{DS(S_{\mathrm{Rect.}}Temp_{MAX})} \cdot 10^N}{Temp_{MAX}})) \cdot V_{out}}{I_{OUT}}\right) \\ &+ \left(\frac{(TEMP_{MAX} \cdot 10^N - (temp_{\mathrm{Real}} \cdot \frac{C_{GS(Temp_{MAX})} \cdot 10^N}{Temp_{MAX}})) \cdot V_{GS}}{I_{OFF}}\right) \end{aligned} \tag{8}$$

$Temp_{MAX}$: *Maximum temperature of MOSFET*
$temp_{Real}$: *Sensed MOSFET temperature*
C_{DS} : *Drain – source capacitance of boost MOSFET at* $Temp_{MAX}$
10^N : *Unit variable of capacitance* (*E.g.* $nF = 10^{-9}$)
I_{ON} : *Gate – on current*
V_{in} : *Input voltage*
V_{out} : *Output voltage*
V_{GS} : *G – S voltage*
I_{IN} : *Input voltage*
I_{OUT} : *Output current*
I_{OFF} : *Gate current*

Control of the equation-predicted dead time produces switch temperature and current/voltage flow in the synchronous boost converter, with which variable control of the dead time can be performed.

4. Result of Experiment

Fig. 8 shows the setup for the experiment performed on the converter of the independent fuel-cell-and-battery hybrid system designed in this study.

The experiment setup consists of a gate drive controller for driving the DSP controller and switching; a full-bridge converter that includes a fuel cell simulator; and a synchronous boost converter. Experiment parameters of

Table 2. Experiment parameters of synchronous boost converter

Parameter.	C_{DS}
Input voltage	30 ~ 50 [V]
Output voltage	40 ~ 55 [V]
Output power	500 [W]
Switching frequency	25 [kHz]
Boost inductor	500 [μH]
Output Capacitor	50 [μF]
Switch	MOSFET

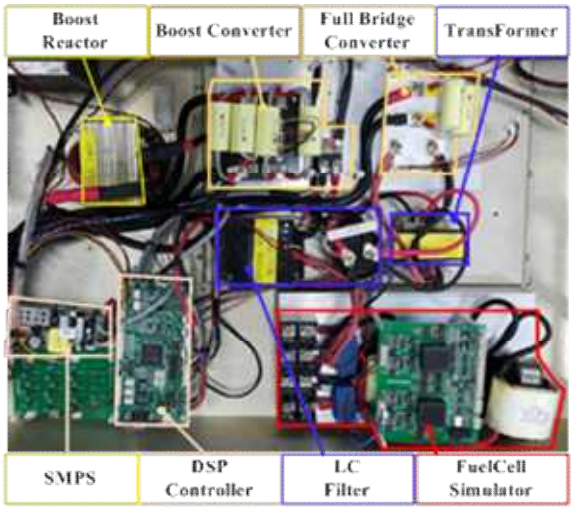

Fig. 8. Experiment setup with a fuel cell simulator

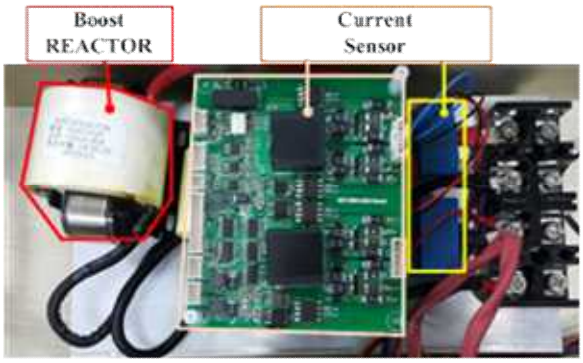

Fig. 9. Image of the fuel cell simulator

synchronous boost converter are as following.

4.1 Fuel cell simulator

Fig. 9 shows the fuel cell simulator. As fuel cell damage can result from arm-short caused by dead time control of a synchronous boost converter or insufficient dead time, a fuel cell simulator was used instead of actual fuel cells, which are costly. The fuel cell simulator controls constant voltage according to the VI characteristic

Fig. 9 shows the configuration of the fuel cell simulator. Control is performed in start mode and dynamic mode according to the output voltage and sensed current. In start mode, voltage is kept at 30V when current of 1A or more flows at the initial 50V, before switching to dynamic mode, in which dynamic control of voltage occurs according to the current level. If discharge current reduces to 1A or less, start mode is restored, and voltage is kept at the initial level of 50V for voltage control corresponding to the fuel cell characteristics. Fig. 10 shows the discharge VI curvature of a DMFC. The simulator was controlled based on the VI discharge curvature of a DMFC. Fig. 11 shows that the VI characteristic of the fuel cell simulator was controlled.

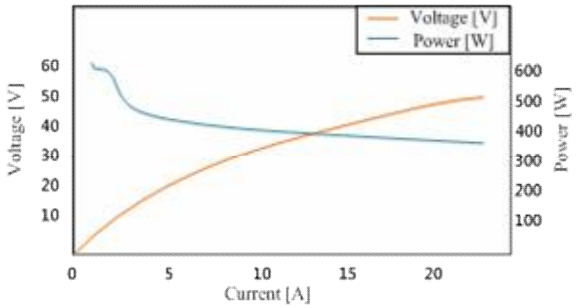

Fig. 10. VI curvature of a DMFC

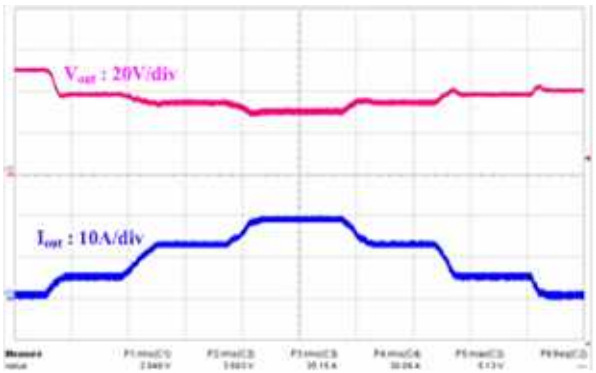

Fig. 11. VI curvature of the fuel cell simulator

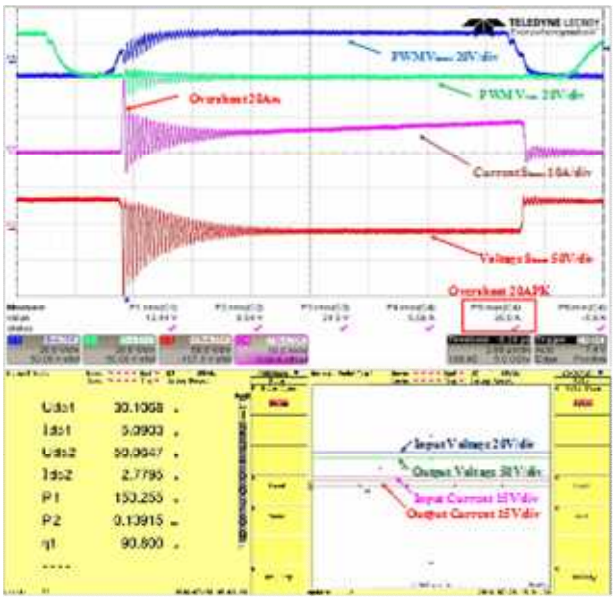

Fig. 12. Waveform of the switch overshoot at the input current of 5.1A

4.2 Synchronous boost converter

Dead time of the complementary switches, S_{boost} and S_{Rect}, in the synchronous boost converter was kept at a consistent value of 2 fs, regardless of the temperature, current, and output voltage.

Fig. 12 shows the waveform of switch voltage and

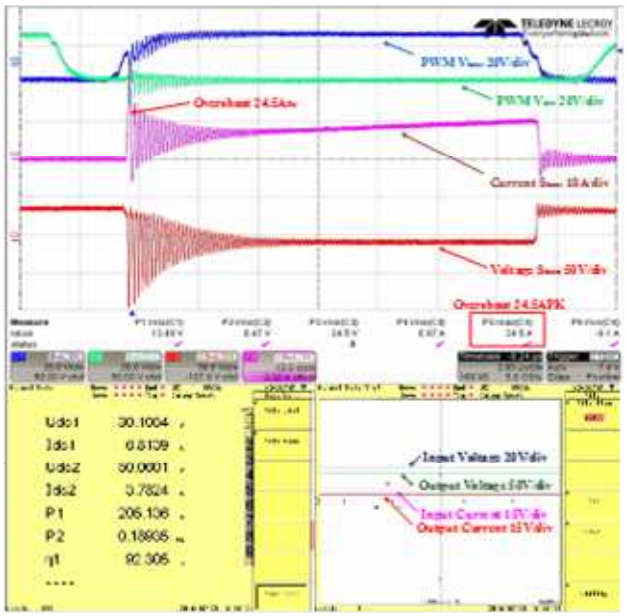

Fig. 13. Waveform of the switch overshoot at the input current of 6.8A

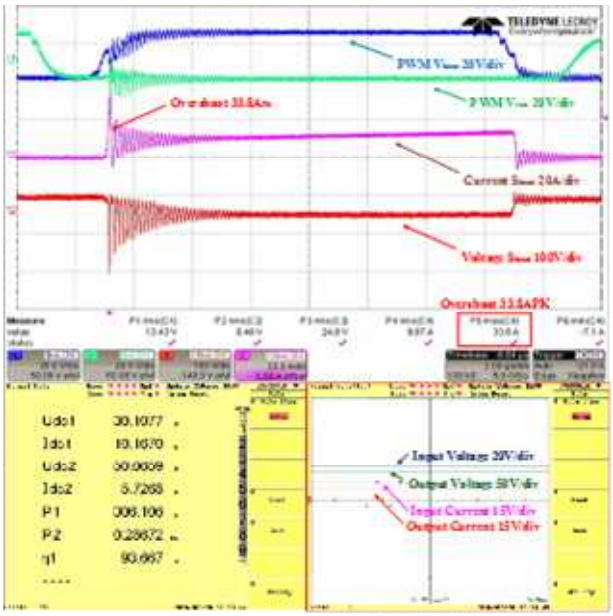

Fig. 15. Waveform of the switch overshoot at the input current of 10.2A

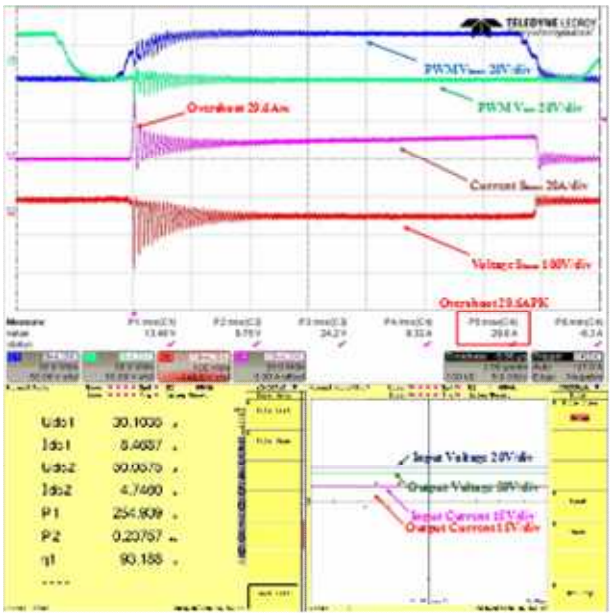

Fig. 14. Waveform of the switch overshoot at the input current of 8.5A

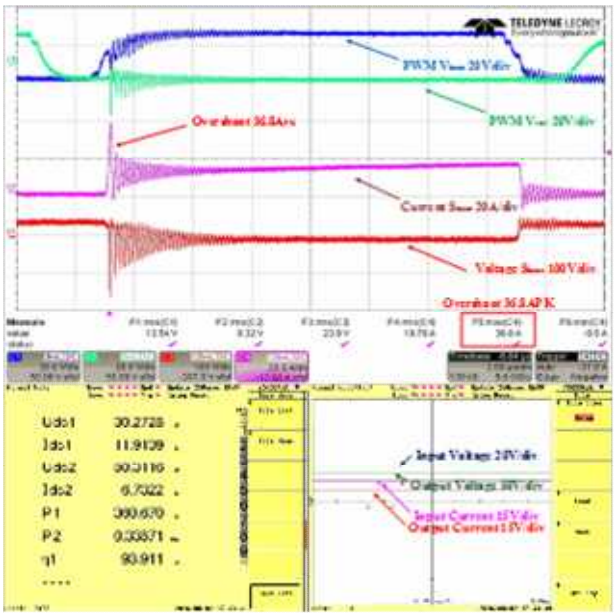

Fig. 16. Waveform of the switch overshoot at the input current of 11.9A

current at the input current of 5.1A. The efficiency of the converter is 90.8%, as the overshoot current is 20A.

Fig. 13 represents the waveform of the switch voltage and current at the input current of 6.8A. The efficiency of the converter is 92.3%, as the overshoot current is 25.5A.

Fig. 14 gives the waveform of the switch voltage and current at the input current of 8.5A. The efficiency of the converter is 93.2%, as the overshoot current is 29.6A.

Fig. 15 shows the waveform of the switch voltage and current at the input current of 10.2A. The efficiency of the converter is 93.7%, as the overshoot current is 33.84A.

Fig. 16 gives the waveform of the switch voltage and current at the input current of 11.9A. The efficiency of the converter is 93.9%, as the overshoot current is 36.8A.

Fig. 17 represents the waveform of the switch voltage and current at the input current of 13.6A. The efficiency of the converter is 94.1%, as the overshoot current is 40.2A. Fig. 18 shows the waveform of the switch voltage and current at the input current of 15.6A. The efficiency of the converter is 94.1%, as the overshoot current is 43.9A.

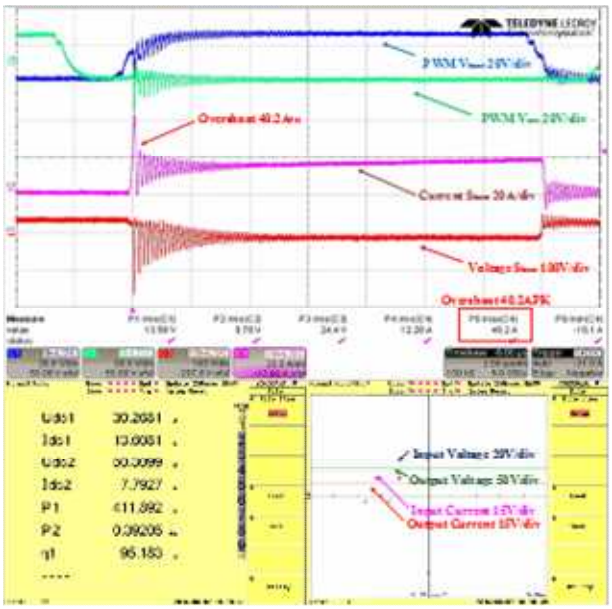

Fig. 17. Waveform of the switch overshoot at the input current of 13.6A

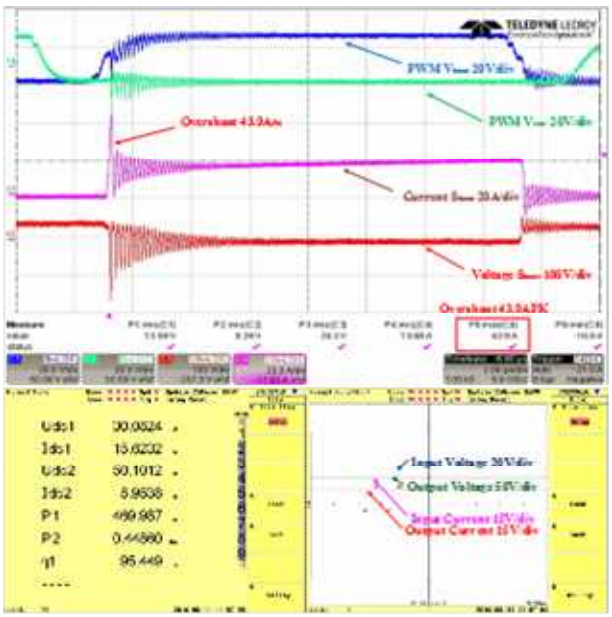

Fig. 18. Waveform of the switch overshoot at the input current of 15.6A

As seen these waveforms, in the conventional method, representing the constant dead time control, the peak current is increased corresponding to the increasing the load.

The peak current of system makes the total system efficiency low. In order to alleviate this problem, the dead time should be readjusted corresponding to the temperature and current. Fig. 19 shows the efficiency curve when the converter uses the conventional fix dead time of 2μs. It is noticeable that the less current is flowing, the less the efficiency.

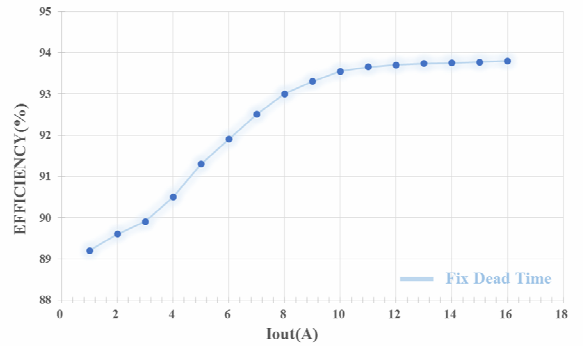

Fig. 19. Efficiency curve of the synchronous boost converter that uses conventional fix dead time

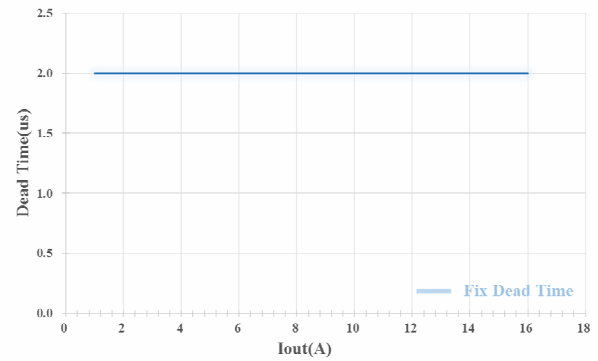

Fig. 20. Relationship between the dead time and current in the conventional constant dead time method

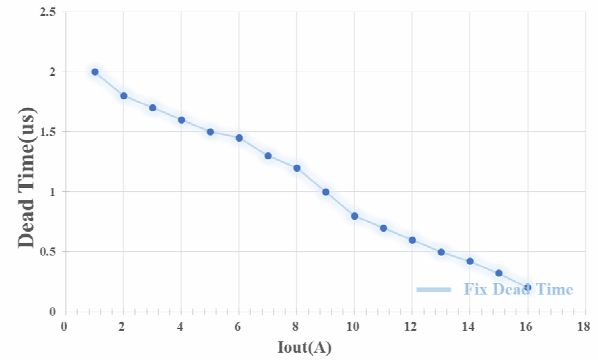

Fig. 21. Relationship between the dead time and current in the proposed method

4.3 Synchronous boost converter with dead time control

Fig. 20 shows the relationship between the dead time and current in the conventional constant dead time method. In the conventional method, the dead time stays constant as the current varies; however, in the dead time predictive method proposed in this paper, the dead time varies along with the current variation as shown in Fig. 21.

Fig. 22 shows the waveform of the switch voltage and current at the input current of 5.1A and dead time of 1.4μs.

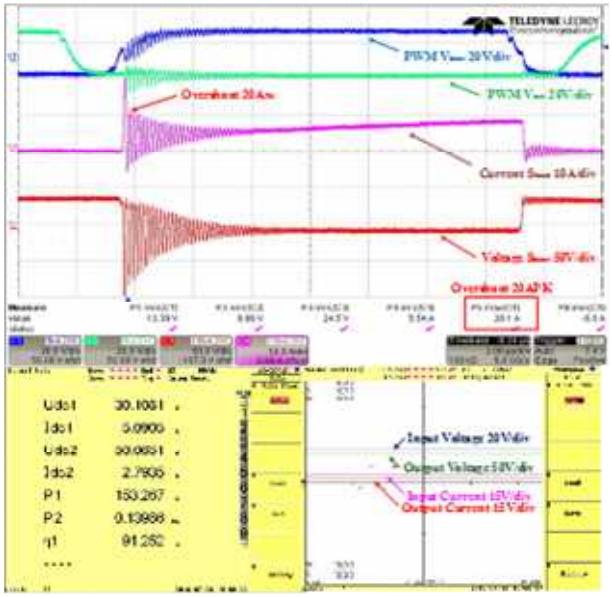

Fig. 22. Waveform of the switch voltage and current at the input current of 5.1A and dead time of 1.4μs

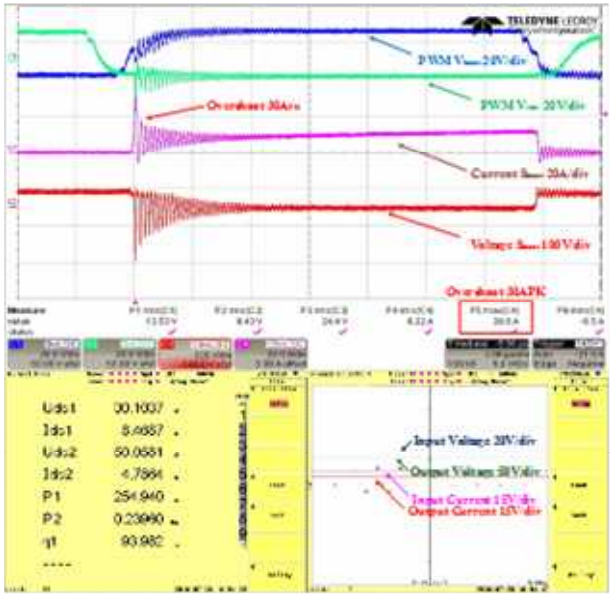

Fig. 24. Waveform of the switch voltage and current at the input current of 8.5A and dead time of 1μs

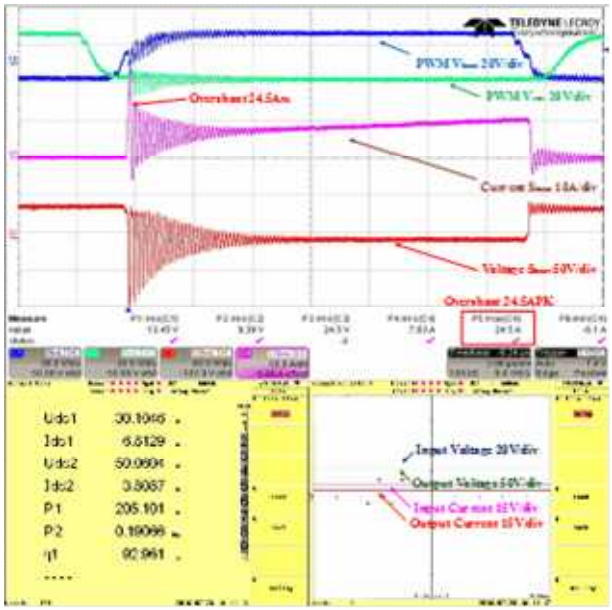

Fig. 23. Waveform of the switch voltage and current at the input current of 6.8A and dead time of 1.2μs

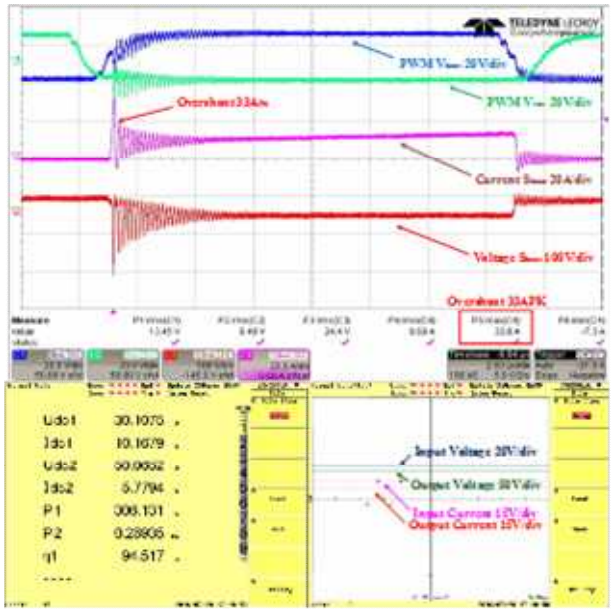

Fig. 25. Waveform of the switch voltage and current at the input current of 10.2A and dead time of 0.8μs

The overshoot current is 20A, the same as the conventional method; however, the efficiency of the converter is 91.3%, improved by 0.5% compared to when the dead time was 2μs.

Fig. 23 shows the waveform of the switch voltage and current at the input current of 6.8A and dead time of 1.2μs.

The overshoot current is 25.5A, decreased by 1A, and the efficiency of the converter is 93%, improved by 0.7% compared to when the dead time was 2μs.

Fig. 24 shows the waveform of the switch voltage and current at the input current of 8.5A and dead time of 1μs. The efficiency of the converter is 94%, which is improved.

Fig. 25 shows the waveform of the switch voltage and current at the input current of 10.2A and dead time of 0.8μs. The overshoot current is 33.4A, and the efficiency of the converter is 94.5%, which is improved.

Fig. 26 shows the waveform of the switch voltage and current at the input current of 11.9A and dead time of 0.6μs. The overshoot current is 36.2A, and the efficiency of the converter is 94.9%, which is improved.

Fig. 27 shows the waveform of the switch voltage and current at the input current of 13.6A and dead time of 0.4μs.

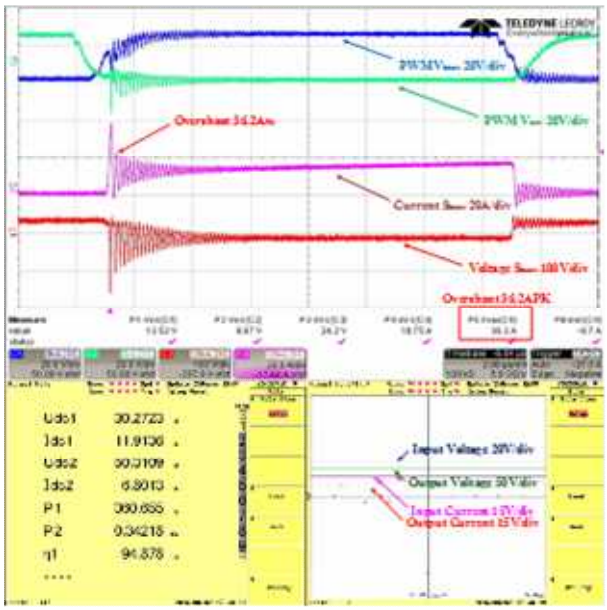

Fig. 26. Waveform of the switch voltage and current at the input current of 11.9A and Dead Time of 0.6μs

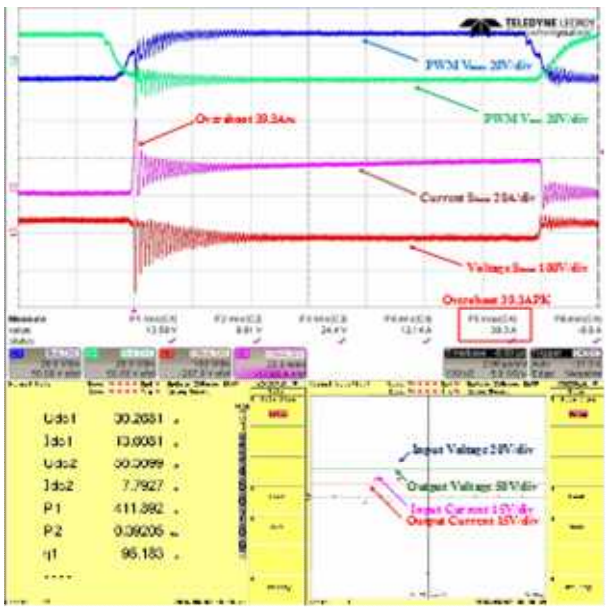

Fig. 27. Waveform of the switch voltage and current at the input current of 13.6A and dead time of 0.4μs

The overshoot current is 39.3A, and the efficiency of the converter is 95.2%, which is improved.

Fig. 28 shows the waveform of the switch voltage and current at the input current of 15.6A and dead time of 0.2μs. The overshoot current is 40.9A, and the efficiency of the converter is 95.4% which is improved.

As a result, it is proven that the proposed method decreases overshoot, and increases its efficiency, compared to the conventional constant dead time method.

Fig. 29 compares the efficiency between the predictive

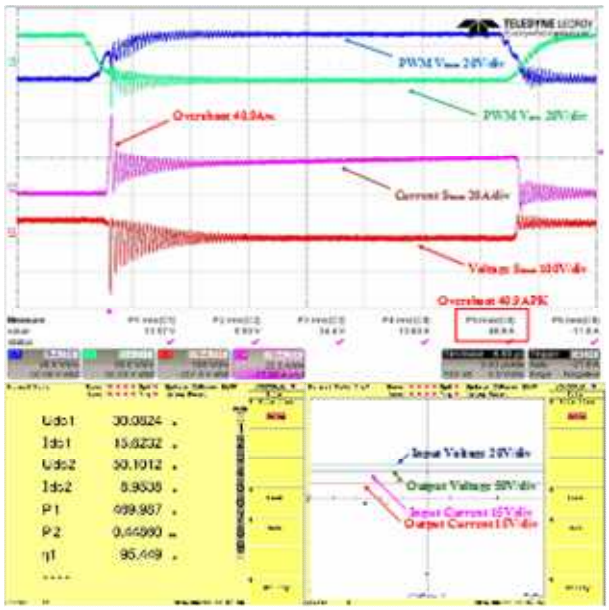

Fig. 28. Waveform of the switch voltage and current at the input current of 15.6A and dead time of 0.2μs

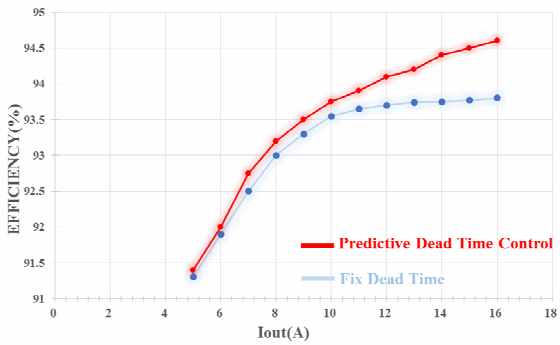

Fig. 29. Efficiency comparison between the predictive dead time control and conventional fix dead time

dead time control and conventional fix dead time. More than 0.5% of efficiency improvement takes place in the high-efficiency of 94% by just implementing predictive dead time control. Greater efficiency improvement is expected when predictive dead time control is implemented where a large current is flowing.

5. Conclusion

This paper explores the design and control of a high-efficiency DC-DC converter with predictive temperature control method in a fuel-cell-and-battery hybrid system.

Our system applies a boost converter for high-efficiency of battery charge, and implements a synchronous boost converter topology using MOSFETs instead of diodes, to reduce loss that occurs by diodes. We propose a method that improves efficiency by 0.5%, by reducing loss that occurs by switching delay that varies by load and tem-

perature, by predicting the ideal dead time from temperature of the component, output voltage, and input current.

Acknowledgements

This research was supported by Basic Science Research Program through the National Research Foundation of Korea(NRF) funded by the Ministry of Education(NRF-2016R1A6A1A03013567)"

This work was supported by the Korea Institute of Energy Technology Evaluation and Planning (KETEP) and the Ministry of Trade, Industry & Energy(MOTIE) of the Republic of Korea. (No. 20162010103830)

References

[1] F. Laurencelle, R. Chahine, J. Hamelin, K. Agbossou, M. Fournier, T. K. Beso, A. Laperriere. "Characterization of a Ballard MK5-E Proton Exchange Membrane Fuel Cell Stack," Fuel Cells Journal, Vol. l, no. l, pp. 66-71, 2001.

[2] Haiping Xu, Gang Ma, Changfu Sun, Xuhui Wen, Li Kong. "Implementation of a bi-directional DC-DC converter in FCEV," *Electrical Machines and Systems*, pp 375-378, Nov, 2003.

[3] R. M. Schupbach, J. C. Balda, "Comparing DC-DC Converters for Power Management in Hybrid Electric-Vehicles," *IEMDC*, pp. 1369-1374, Jun. 2003.

[4] Jong-Soo Kim, Gyu-Yeong Choe, Byoung-Kuk Lee, Jae-Sun Shim, "Advanced Interchangeable Dynamic Simulation Model for the Optimal Design of a Fuel Cell Power Conditioning System," *J. of Electrical Engineering & Technology*, Vol. 5, No. 4, pp. 561-570, 2010.

[5] G. Graditi; G. Adinolfi, "Comparative Analysis of Syn-chronous Rectification Boost and Diode Rectification Boost Converter for DMPPT Applications," *IEEE In-ternational Symposium, Industrial Electronics*, Jun 2011.

[6] Nguyen Van Sang, "Non-isolated Boost Charger for the Li-Ion Batteries Suitable for Fuel Cell Powered Laptop Computers," *J. of Power Electronics*, Vol. 13, no. 1, pp. 31-39, 2013.

[7] Tai-Sik Hwang and Sung-Yeul Park, "Seamless Boost Converter Control Under the Critical Boundary Condition for a Fuel Cell Power Conditioning System," *IEEE Transactions on Power Electronics*, Vol. 27, no. 8, Aug 2012.

[8] Jong-Soo Kim, Gyu-Yeong Choe, "An Optimal Design Methodology of an Interleaved Boost Converter for Fuel Cell Applications," *J. of Electrical Engineering & Technology*, pp. 561-570, 2010.

[9] Boumediène ALLAOUA, Abdellah LAOUFI "Application of a Robust Fuzzy Sliding Mode Controller Synthesis on a Buck-Boost DC-DC Converter Power Supply," J. of Electrical Engineering & Technology Vol. 6, No. 1, pp. 67-75, 2011.

[10] Sang-Ho Moon, Sung-Tak Jou, Kyo-Beum Lee "Performance Improvement of a Bidirectional DC-DC Converter for Battery Chargers using an LCLC Filter," *J. of Electrical Engineering & Technology,* Vol. 10, No. 2, pp. 560-573, 2015.3.

[11] Bong-Gi You, Jeong-Min Ko, Jun-Hyung Kim, Byoung-Kuk Lee, "Proposal of Potted Inductor with Enhanced Thermal Transfer for High Power Boost Converter in HEVs," *J. of Electrical Engineering & Technology,* Vol. 10, No. 3, pp. 1075-1080, 2015.5.

[12] Anbukumar Kavitha, Govindarajan Uma "Resonant Parametric Perturbation Method to Control Chaos in Current Mode Controlled DC-DC Buck-Boost Converter," *J. of Electrical Engineering & Technology* Vol. 5, No. 1, pp. 171-178, 2010.3.

[13] Vijayalakshmi, S, Sree Renga Raja, T "Time_Domain_Based_Digital_Controller_for_Buck-Boost_ Converter" *J. of Electrical Engineering & Technology,* Vol. 9, No. 5, pp.1551-1561, 2014.9.

[14] Stefan Waffler, Johann W. Kolar, "A Novel Low-Loss Modulation Strategy for High-Power Bidirectional Buck+Boost Converters," *IEEE Trans. Power Electron*, vol. 24, no. 6, pp. 1589-1599, Jun. 2009.

[15] Abdul Motin Howlader, Naomitsu Urasaki, "Optimal PAM Control for a Buck Boost DC-DC Converter with a Wide-Speed-Range of Operation for a PMSM," *J. of power electronics*, Vol. 10, no. 5 pp. 491-497, 2010.

Do-Yun Kim He received the B.S. degree in electrical and electronic engineering from Anyang University, Anyang, Korea, in 2011, and the M.S degree in 2013 in interdisciplinary program in energy system engineering and the Ph.D. degree in interdisciplinary program in photovoltaic system engineering at Sungkyunkwan University, Suwon, Korea. Since 2017, he has been a Senior Research Engineer at LG Electronics, Incheon, Korea. His research interests include inverter and battery management system and its robust control.

Il-Kuen Won He received the B.S. degree in electrical and electronic engineering from Sungkyunkwan University, Suwon, Korea, in 2013. He is currently working toward the Ph.D. degree in electrical and computer engineering at Sungkyunkwan University, Suwon, Korea. His research

interests include inverter, motor control and battery systems.

Jung-Hyo Lee He received the B.S. degree in electrical engineering from Konkuk University, Seoul, Korea, in 2006, and the M.S. and the Ph.D. degrees in electrical engineering from Sungkyunkwan University, Suwon, Korea, in 2008 and 2013, respectively. From 2013 to 2016, he was a senior researcher of automotive component R&D Team in LG Innotek. From 2016, he has been an assistant professor in Kunsan National University, Gunsan, Korea. His research interests include converters and inverters for motor drive application.

Chung-Yuen Won He received B.S. degree in electrical Engineering from Sungkyunkwan University, Suwon, Korea, in 1978, and the M.S. and Ph.D. degrees in Electrical Engineering from Seoul National University, Seoul, Korea, in 1980 and 1987, respectively. From 1990 to 1991, he was with the Department of Electrical Engineering, University of Tennessee, Knoxville, TN, USA as a Visiting Professor. Since 1988, he has been with a member of the faculty of Sungkyunkwan University, where he is a Professor in the College of Information and Communication Engineering; also, in 2008-2013, he was the director of Samsung Energy Power Research Center. He was the President of the Korean Institute of Power Electronics in 2010. Since 2016, he has been a director of the DC distribution research center. His current research interests include the power electronic of electric machines, electric / hybrid vehicle drives, power converters for renewable energy systems. He is a member of the Korea Institute of Power Electronics.